A Novel 3D Strain-Adaptive Continuum Orthotropic Bone Remodelling Algorithm: Prediction of Bone Architecture in the Femur

D.M. Geraldes and A.T.M. Phillips

Structural Biomechanics Group, Dept. Civil and Environmental Engineering, Imperial College London, United Kingdom

Abstract— **Prediction of trabecular architectural arrangement and bone property distribution is fundamental in understanding the underlying mechanics of fractures. An iterative strain-adaptive bone remodelling algorithm that predicts orthotropic elastic property distribution in bone was developed and applied to a three-dimensional (3D) model of the proximal femur. Bone was modelled as a continuum matrix with local orthotropic material properties. In each iterative step, local material orientations were updated in order to match the principal stress directions and local properties modified according to the associated normal strains. The model was run iteratively until convergence was achieved. Results showed that the proposed algorithm could predict known trabecular features and architecture. Directionality of these trabecular structures matched previously observed primary and secondary compressive and tensile groups in the proximal femur. Currently, more physiologically accurate models of the whole femur are being developed, with inclusion of free boundary conditions and multiple load cases. It is believed that this approach can be a valuable tool in assessing directionality of bone structure and corresponding orthotropic material property distribution. It can have a direct impact on the understanding of fracture mechanics and development of impact protection devices for vehicle collisions or high risk roles, amongst other applications.**

Keywords — **Bone Remodelling, Orthotropic Properties, Proximal Femur, Directionality, Fracture Prediction.**

I. Introduction

Recently, finite element models that simulate bone response to its mechanical environment have been developed. These allow prediction of bone remodelling or morphogenesis to altered load conditions, such as during the fracture healing process and in bone-implant interactions [1,2]. In order to simplify the analysis and reduce computational times, bone is usually considered to have isotropic properties. This isotropic material assumption does not explain the directionality observed in bone's internal trabecular structures [3,4], as well as the orthotropic properties that have been verified in other studies [5,6]. Orthotropy has been shown to be a close approximation to bone's anisotropy [7]. Prediction of stiffness distribution and directionality in bone structures can be a very important tool in understanding the mechanics underlying fracture initiation and propagation [8]. 2D modelling of the femoral head with orthotropic bone properties and adaptation of its structure to match local stimuli has been demonstrated to produce a good match with the trabecular orientation of the bone in its physiological state [9,10]. Because trabecular structures in the proximal femur are well documented [5,11] and have been observed via imaging techniques, such as *in vivo* radiographs or CT scans [12] and *ex vivo* bone slices, it was decided that the orthotropic strain-adaptive bone remodelling algorithm should be firstly developed and validated for this region with its results compared to the structures observed *in vivo*. This paper describes a novel iterative algorithm to predict 3D distribution and orientation of material properties, with bone considered as an orthotropic strain-driven adaptive continuum. It is hypothesised that the fully developed approach can lead to the production of an accurate stiffness and directionality prediction tool, which will allow more thorough understanding of bone fracture mechanics. Research in areas such as impact protection devices and protective clothing can be improved through the use of orthotropic heterogeneous models, allowing assessment of directionally dependent strain fields.

II. Methods

This iterative algorithm uses Abaqus (v.6.9, SIMULIA, Dassault Systèmes), MATLAB (vR2007b, MathWorks) and Python (v.2.5., Python Software Foundation). It was developed with simplified 2D and 3D models before being applied to the proximal femur [10].

A. The Bone Remodelling Algorithm

At each iteration, n, every element's strains and stresses were extracted (Python) from the Abaqus output database and processed (MATLAB). The element material orientations were matched with the local principal stress orientations, N (Equation 1) and their associated strain stimuli, ε', found (Equation 2),

$$\left[N\ \sigma_p\right] = \mathrm{eig}(\sigma) \tag{1}$$

C.T. Lim and J.C.H. Goh (Eds.): WCB 2010, IFMBE Proceedings 31, pp. 772–775, 2010.
www.springerlink.com

$$\varepsilon' = N^T \varepsilon N \quad (2)$$

where ε and ε' are the reported and transformed strain stimuli, respectively. The elements outside the remodelling plateau (Table 1) were then updated proportionally to the absolute value of their associated strains in order to achieve a target strain value of 1250 μstrain [13] (Equation 3),

$$E_n = E_{n-1} \times \frac{\varepsilon\prime}{1250} \quad (3)$$

with E_n limited between 10 MPa and 20 GPa [7,14]. E_1, E_2 and E_3 were based on the normal strains associated with the minimum, medium and maximum principal stresses, respectively. Poisson's ratios, ν_{ij}, were calculated (Equation 4) [15], and shear moduli, G_{ij}, taken as a constant fraction of the average of the Young's Moduli (Equation 5) [16],

$$\frac{\nu_{ij}}{\nu_{ji}} = \frac{E_i}{E_j} < 0.09 \ , \qquad G_{ij} = \frac{E_i + E_j}{4} \quad (4,5)$$

The model was considered to achieve a state of convergence when E_1, E_2 and E_3 remained constant at less than ±5% between iterations for at least 95% of elements and the change in the model average elastic moduli values was less than ±1% after the tenth iteration.

Table 1 Strain limits for different bone remodelling actions [13]

Action	Threshold (μstrain)
Bone Weight Reduction	100-1000
Remodelling Plateau	1000-1500
Bone Weight Increase	1500-3000

B. The Model

The geometry for the proximal femur was extracted from a Sawbones synthetic model (60 year old Caucasian male, 183cm, 91kg). The femoral head was meshed with 139580 tetrahedral C3D4 elements with the same initial orthotropic material orientations (aligned with the global axis system) and properties (Young's Modulus, Shear Modulus and Poisson's ratio). All elements were modelled with the initial material properties described in Table 2.

The surface of the distal end of the diaphysis was fixed against translation in the vertical direction with a node in the medial cortex fixed against translation in all directions and a node in the lateral cortex fixed against posterior-anterior translation. The femoral head was loaded with a single set of simplified load forces at 10% of the gait cycle (Table 3), with the joint reaction force (JRF), the abductor muscle group (AbG) and the ilio-tibial tract (ITT) included as point loads.

Table 2 Initial material properties

Engineering Constant	value
E1, E2, E3	10 MPa
G_{12}, G_{13}, G_{23}	5 MPa
ν_{12}, ν_{13}, ν_{23}	0.3

Table 3 Summary of the total forces applied and their components (N)

Force	Total	X-axis	Y-axis	Z-axis
JRF	2500	536.4	361.8	2414.8
AbG	1250	427.5	0	1174.6
ITT	625	0	0	625.0

III. Results

After convergence (11th iteration), coronal slices of the proximal femur showing the stiffness distributions and their correspondent material orientations were produced. Following convergence as expected, the principal strain directions were aligned with the principal stress directions.

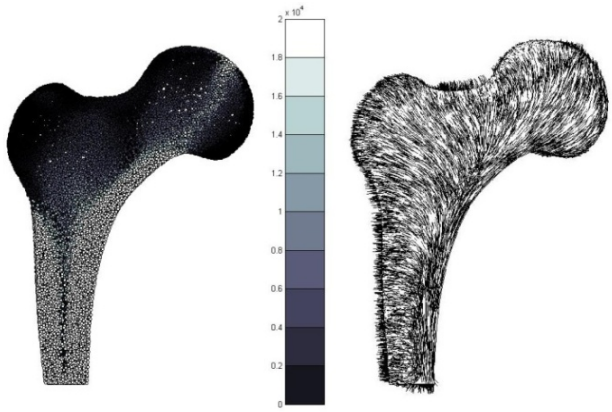

Fig. 1 Stiffness distribution plot for E_1 (associated with minimum principal stresses) in MPa (left) and associated orientations (right)

In Figure 1, E_1 orientations fan out from the internal diaphysis both towards the great trochanter and the load point on the femoral head. The presence of the primary compressive group [11] is seen as dense high stiffness elements arching from the medial aspect of the shaft of the femur towards the upper portion of the femoral head. The

secondary compressive group [11] appears as less dense, more disperse high stiffness values arching from the medial aspect of the shaft towards the great trochanter.

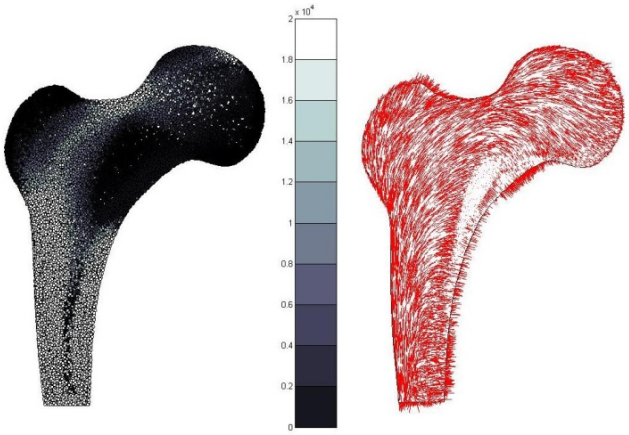

Fig. 2 Stiffness distribution plot for E_3 (associated with maximum principal stresses) in MPa (left) and its associated orientations (right)

In Figure 2, E_3 orientations describe an arch through the femoral neck and epiphysis, connecting the lateral diaphysis with the medial diaphysis and the great trochanter. Below the contact region with the acetabulum and the Ward's triangle in the femoral neck, E_3 directions rotate into the posterior-anterior plane, as a result of the direction of the JRF applied. The presence of the primary tensile group can be observed as a dense high stiffness value zone arching from the lateral shaft of the femur across the femoral neck towards the femoral head [11]. The secondary tensile group can also be seen as a less dense, more disperse region of high stiffness elements immediately below the primary tensile group, arching from the lateral shaft across the midline of the femur [11]. Along the great trochanter, a region with elements of medium stiffness values matching the arrangement of the great trochanter group arose [11].

As one would expect, the stiffness distribution for E_{mean}, the arithmetic average of E_1, E_2 and E_3 for each element, corresponds to a superposition of Figures 1 and 2 (Figure 3). Primary and secondary compressive and tensile groups are clearly present with a less evident great trochanter group also shown. The femoral shaft has elements of stiffness values within the range found for cortical bone (16 – 20 GPa) and the intermedullary canal resembles the expected femoral construct, although reduced in diameter. Finally, a region with minimum stiffness values corresponding to the Ward's triangle is also observed. This coronal representation of the proximal femur shows good correlation and resemblance with the *in vivo* trabecular architecture and distribution in the proximal femur.

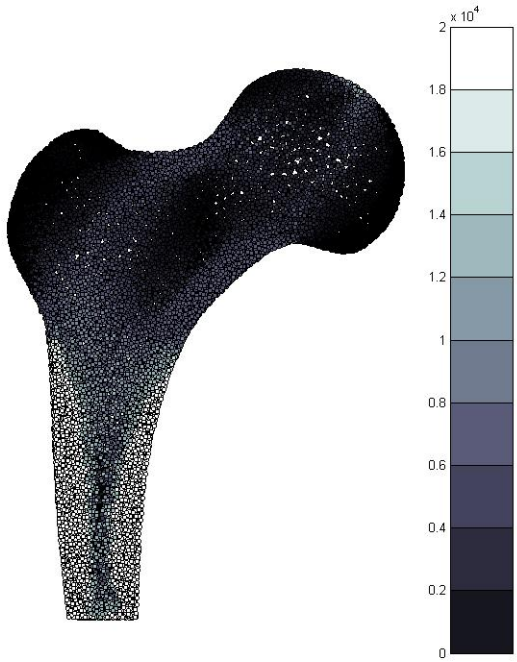

Fig. 3 Stiffness distribution plot for E_{mean}

IV. Discussion and Conclusion

The areas where medium or high values for E_{mean} (Figure 3) can be found are below the great trochanter, along the lateral epiphysis, in the femoral head and along the surface of the diaphysis. These are areas of high compression or tension stresses due to bending of the proximal femur because of the action of the muscle groups and the application of the JRF [5,17]. The lower value regions observed are known for being composed of thin and loosely arranged trabeculae, which imply a lower stiffness distribution [11]. The lack of stiffness in this region might explain the frequent occurrence of femoral neck fractures, as any increase of stress applied off the natural loading direction will meet low directional stiffness values, increasing the probability of fracture. E_{mean} distribution shows good correlation with the observed *in vivo* structures [5,17] with the zones of expected high stiffness (trabecular groups and cortical femoral shaft) and of low stiffness (Ward's triangle and intermedullary canal) arising. However, the femoral shaft and intermedullary canal do not arise as clearly as expected. It is hypothesised this is due to the fixed boundary conditions applied at the distal end, increasing the bending moment in the diaphysis compared to the physiological situation. The local orientation plots show that both the great trochanter, the primary and secondary compressive and tensile trabeculae groups are predicted. In the E_1 plot (Figure 1), a slightly

curved group of closely packed trabeculae originating in the medial cortex of the femoral shaft and ending in the upper part of the femoral head (primary compressive group) and a spaced trabecular group arising below the principal compressive group in the medial cortex of the femoral shaft and ending by the great trochanter (secondary compressive group) can be seen [11]. The E_3 plot (Figure 2) shows that the three tensile groups are also present: trabeculae originating in the lateral cortex below the great trochanter and ending at its surface (great trochanter group), a group of trabeculae starting in the lateral cortex below the great trochanter in the lower part of the femoral head and curving upwards and inwards across the neck of the femur (primary tensile group) and trabeculae originating below the primary tensile group in the lateral cortex, arching upwards and medially across the upper end of the femur and ending irregularly after crossing the midline (secondary tensile group) [11]. The model also suggests that material properties are not oriented only in the coronal plane, but they can be projected into other planes (Figure 2). This twisting of the primary tensile group is seen to provide an efficient load path to carry the JRF and AbG forces to the cortex.

The proposed algorithm qualitatively predicts stiffness distribution and material property orientations in bone. However, there are limitations to this method, such as the use of fixed boundary conditions and the inclusion of a single load case and simplified load sets applied as point loads. The addition of combined load cases, representing a greater envelope of stress peaks generated by routine daily activities (standing up, sitting down, climbing stairs), more muscle groups applied in insertion zones instead of nodes and free boundary conditions [18] (more representative of the *in vivo* case than the fixed boundary conditions used in this study) is currently being undertaken for a whole femur construct. It is believed this will lead to a more accurate and physiologically representative prediction of bone architecture. Validation of this model will then take place by comparing extracted directionality information from the model with both *ex vivo* bone samples and *in vivo* imaging data.

Stiffness distribution and bone structure directionality can be assessed by considering bone to have orthotropic material properties that respond proportionally to directional strain stimuli. Currently, more physiological models are being developed in order to approach the results to the *in vivo* situation. It is hypothesised that the developed stiffness and directionality distribution tool will lead to a more thorough understanding of the mechanics underlying bone fractures. The models developed using this tool can be applied in research areas such as impact protection allowing increased information on how fractures arise and the likelihood of certain fracture types under specific conditions.

References

1. Huiskes R, Weinans H et al. (1987) Adaptative bone-remodelling theory applied to prosthetic-design analysis. J Biomech 20(11/12):1135-1150
2. Turner C, Anne V et al. (1997) A uniform strain criterion for trabecular bone adaptation: do continuum-level strain gradients drive adaptation? J Biomech 30(6):555-563
3. Dalstra M, Huiskes R et al. (1993) mechanical and textural properties of pelvic trabecular bone. J Biomech 26(4/5):523-535
4. Wolff J (1892) The law of bone remodelling (Translated by Maquet P, Furlong R). Berlin, Heidelberg, Springer-Verlag
5. van Rietbergen B, Odgaard A et al. (1998) Relationships between bone morphology and bone elastic properties can be accurately quantified using high-resolution computer reconstructions. J Ortho Res 16:23-31
6. Yang G, Kabel J et al. (1999) The anisotropic hooke's law for cancellous bone and wood. J Elasticity 53:125-146
7. Ashman R, Cowin S et al. (1984) A continuous wave technique for the measurement of the elastic properties of cortical bone. J Biomech 17:349-361
8. Reilly G and Currey J (1999) The development of microcracking and failure in bone depends on the loading mode to which is adapted. J Exp Biology 202:543-552
9. Miller Z, Fuchs M et al. (2002) Trabecular bone adaptation with an orthotropic material model. J Biomech 35:247-256
10. Geraldes D, Phillips ATM (2009) Development of a continuum and free boundary condition model of the pelvis for acetabular fracture pattern prediction. International Society of Biomechanics, Cape Town, South Africa 2009
11. Singh M, Nagrath AR et al. (1970) Changes in trabecular pattern of the upper end of the femur as an index of osteoporosis. J Bone Joint Surg 52:457-467
12. Tsubota K, Suzuki Y et al. (2009) Computer simulation of trabecular remodeling in human proximal femur using large-scale voxel fe models: Approach to understanding wolff's law. J Biomech 42:1088-1094
13. Frost H (1987) Bone 'mass' and the 'mechanostat': A proposal. Anat Record 219:1-9
14. Rho JY, Kuhn-Spearing L et al. (1998) Mechanical properties and the hierarchical structure of bone. Med Eng & Phys 20:92-102
15. Cowin S, van Buskirk W (1986) Technical note: thermodynamic restrictions on the elastic constants of bone. J Biomech 19:85-88
16. Ford C, Keaveny T (1996) The dependence of shear failure properties of trabecular bone on apparent density and trabecular orientation. J Biomech 29(10):1309-1317
17. Skedros J, Baucom S (2007) Mathematical analysis of trabecular 'trajectories' in apparent trajectorial structures: The unfortunate historical emphasys on the human proximal femur. J Theo Biol 244:15-45
18. Phillips ATM (2009) The femur as a musculo-skeletal construct: A free boundary condition modeling approach. Med Eng & Phys 31:673-680

Author: Diogo Geraldes
Institute: Imperial College London
Street: Room 223, Dept. Civil and Environmental Engineering, Imperial College London, Exhibition Road, SW7 2AZ
City: London
Country: United Kingdom
Email: geraldes@imperial.ac.uk